Journal of Nanofluids
Vol. 6, pp. 362–367, 2017
(www.aspbs.com/jon)

ARTICLE

Forced Convection Heat Transfer of Nanofluids in a Channel Filled with Porous Media Under Local Thermal Non-Equilibrium Condition with Three New Models for Absorbed Heat Flux

T. Armaghani[1], M. J. Maghrebi[2], A. J. Chamkha[3,4,*], and A. F. Al-Mudhaf[5]

[1]Department of Engineering, Mahdishahr Branch, Islamic Azad University, Mahdishahr, 3561875915, Iran
[2]Department of Mechanical Engineering, Ferdowsi University of Mashhad, Mashhad, 9177948974, Iran
[3]Mechanical Engineering Department, Prince Mohammad Bin Fahd University, Al-Khobar 31952, Kingdom of Saudi Arabia
[4]Prince Sultan Endowment for Energy and Environment, Prince Mohammad Bin Fahd University, Al-Khobar 31952, Saudi Arabia
[5]Manufacturing Engineering Department, The Public Authority for Applied Education and Training, Shuweikh 70654, Kuwait

The present work considers forced convection heat transfer of nanofluids in a channel filled with porous media under the Local Thermal Non-Equilibrium (LTNE) condition and includes a *three-equation energy model*, for the fluid/particle/solid phases. The fully-developed flow and the steady Darcy-Brinkman equation is employed in the porous medium channel. The local thermal non-equilibrium model is assumed between the fluid, particles and the solid phases. The nanoparticles are considered with a non-uniform distribution inside the channel. As a result, the volume fraction distribution equation is also coupled with the other governing equations. The effects of the Nield number and the modified thermal capacity ratio on the heat transfer are completely studied. In our previous work, we introduced one model for calculating the absorbed heat flux by solid, particle and fluid phases. In this paper, three new different heat flux models are proposed and compared together. The effect of Nield number on absorbed heat flux obtained by 4 models are completely studied and compared together.

KEYWORDS: Nanofluids, Porous Media, Absorbed Heat Flux, Nield Number, Conductivity Ratio.

1. INTRODUCTION

The present work is an extension to our previous work on convection heat transfer of nanofluids in a channel filled with porous media (see Maghrebi et al.[1] Armaghani et al.[2,3] and Nazari et al.[4]). Nanofluids is a name conceived by Choi[5] at Argonne National laboratory and corresponds to fluids consisting of solid nanoparticles with size less than 100 nm suspended with solid volume fraction typically less than 4%. Nanofluid can enhance heat transfer performance compared to pure liquids. Nanofluids can be used to improve thermal management system in many engineering application such as transportation, micromechanics and instrument and cooling devices. Recently, many investigators studied nanofluid convective heat transfer in different geometry both numerically and experimentally.[6–10] For numerical simulation, two approaches have been adopted in the literature to investigate the heat transfer characteristics of nanofluids, namely, the single-phase model and the two-phase model. Another approach is to adopt the Boltzmann theory.[11] In single-phase model, a uniform volume fraction distribution is assumed for nanofluids. In other words, the viscosity and thermal conductivity of nanofluids are formulated by volume fraction and nanoparticle size then continuity, momentum and energy equations are solved for nanofluids. In the two-phase model, the volume fraction distribution equation is added to other conservation equations. Many investigators used the single- and the two-phase models for investigating the flow and heat transfer of nanofluids.[12–16]

Buongiorno[17] introduced seven slip mechanisms between nanoparticles and the base fluid. He showed that the Brownian motion (movement of nanoparticles from high concentration site) and thermophoresis (movement of nanoparticles from the high temperature site to the low temperature site) have effected significantly in the laminar forced convection of nanofluids. Based on this finding, he developed non-homogeneous two-component equations

*Author to whom correspondence should be addressed.
Email: achamkha@yahoo.com
Received: 7 October 2016
Accepted: 22 November 2016

 2169-432X/2017/6/362/006 doi:10.1166/jon.2017.1323

in nanofluids. Heyhat and Kowsary[18] used Buongiorno's model for investigating the effect of particles migration on flow and convective heat transfer of nanofluids flowing through the circular pipe. Results show that the non-uniform distribution leads to a higher heat transfer coefficient while the wall shear stress is decreased. Therefore, the particle migration can play an important role in improvement of the heat transfer coefficient in convective heat transfer in nanofluids. Recently, Saryazdi et al.[19] numerically investigated forced convection flow and heat transfer of a nanofluid flowing inside a straight circular pipe filled with a saturated porous medium under LTE condition using Buongiorno's model.

The effect of local thermal non-equilibrium on the onset of convection in a nanofluid and thermal instability in a porous medium layer saturated by a nanofluid are investigated by Nield and Kuznetsov.[20,21] They pointed in these papers it is assumed that no nanoparticle agglomeration occurs and that the nanoparticle suspension remains stable. According to Anoop et al.,[22] there are experimental techniques that make it possible to prepare nanoparticle suspensions that remain stable for several weeks. They treat the nanofluid as a continuum, using quantities averaged over a representative elementary volume, a procedure common in the study of flow in a saturated porous medium. In recent papers, written by Kuznetsov and Nield[23–25] the Buongiorno's model was applied to the Horton-Rogres-Lapwood problem (the onset of convention in a horizontal layer of a porous medium uniformly heated from below). Both Brownian motion and thermophoresis give rise to cross-diffusion terms that are in some way analogous to the familiar Soret and Dufour cross-diffusion terms that arise with a binary fluid. Nield and Kuznetsov[26] introduced an analytical treatment of double-diffusive natural convection boundary layer flow in a porous medium saturated by nanofluid. They used the Buongiorno's model for modeling the nanofluid and Darcy model for porous medium. The result showed a decrease in the reduced Nusselt number associated with an increase in the thickness of the thermal boundary layer an increase in Brownian motion parameter, buoyancy ratio, thermophoresis parameter, modified Dufour parameter and a decrease in regular buoyancy ratio. The analytical treatment of double-diffusive natural convection boundary layer flow of a nanofluid past a vertical plate was also studied by Kuznetsov and Nield.[27]

The effects of particle migration on forced convective heat transfer of nanofluid in a porous medium are investigated by Maghrebi et al.[1] They show the particles migration has a significant role in heat transfer. The results show that the local Nusselt number is decreased when the Lewis number is increased. It is observed that as the Lewis number is increased, the wall temperature gradient is decreased and as a consequence the local Nusselt number is decreased. The effects of Lewis number, Schmidt number and modified diffusivity ratio on the volume fraction distribution are also studied and discussed. In the recent papers written by Armaghani et al.,[2] the effects of particle migration in a porous channel on nanofluid convective heat transfer are completely studied when the assumption of local thermal non-equilibrium is valid between the phases. Armaghani et al.[3] investigated the effects of Nield number on nanofluid forced convection heat transfer on the porous channel under local thermal non-equilibrium condition. They also introduced one model for considering the absorbed heat flux. New models for heat flux splitting at the boundary of a porous medium: three energy equations for nanofluid flow under local thermal Non-Equilibrium condition investigated by Nazari et al.[4] They proposed three heat flux models for the first time. The proposed models are also compared together and analyzed.

In this paper, we extend our research about nanofluid forced convection heat transfer on the porous channel under local thermal non-equilibrium condition and propose 3 new models for obtaining the absorbed heat flux. The models are completely discussed and compared together also the effects of Nield number on absorbed heat flux obtained by 4 models are completely studied and compared together. The effect of conductivity ratio on solid temperature distribution is studied too.

2. MATHEMATICAL FORMULATION

The forced convection heat transfer in a two-dimensional channel is investigated by solving the mathematical formulations introduced in this section numerically. The channel is occupied with a saturated porous medium. Figure 1 shows the schematic of the porous channel and the system coordinates. The nanofluids (Al_2O_3 or TiO_2, etc.) which is treated as a two-component mixture, is flown in the channel as discussed by Buongiorno.[17] The governing equations for forced convection heat transfer of nanofluid in saturated porous medium under local thermal Non-Equilibrium condition are presented in previously papers such as Nazari et al.[4]

The dimensionless forms of mentioned equations are:

$$\nabla^2 u^* - \frac{u^*}{Da} - \frac{1}{Da}\frac{dP^*}{dx^*} = 0 \tag{1}$$

$$\frac{\partial T_f^*}{\partial t^*} + u^*\frac{\partial T_f^*}{\partial x^*} = \frac{1}{Re\,\mathrm{Pr}}\Big[\nabla^2 T_f^* + \frac{\tau}{Le}(\nabla\varphi^*\cdot\nabla T^*) + \frac{\tau}{LeN_{bt}}(\nabla T_f^*\cdot\nabla T_f^*) + N_{hp}(T_p^* - T_f^*) + N_{hs}(T_s^* - T_f^*)\Big] \tag{2}$$

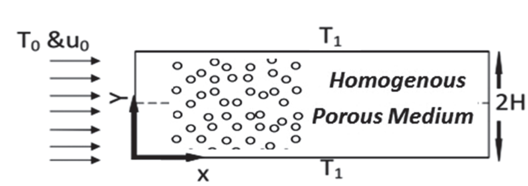

Fig. 1. Geometry of problem and system of coordinate.

$$\frac{\partial T_p^*}{\partial t^*}+\frac{1}{\varepsilon}u^*\cdot\nabla T_p^* = \frac{1}{Re\Pr}[\varepsilon_p\nabla^2 T_p^*+\gamma_p N_{hp}(T_f^*-T_p^*)] \quad (3)$$

$$\frac{\partial T_s^*}{\partial t^*} = \frac{1}{Re\Pr}[\varepsilon_s\nabla^2 T_s^*+\gamma_s N_{hs}(T_f^*-T_s^*)] \quad (4)$$

It is obvious that at steady-state condition, the Péclet number doesn't play any role in the solid-phase temperature. The particle volume fraction equation can be expressed as,

$$\frac{\partial \varphi^*}{\partial t^*}+\frac{1}{\varepsilon}u^*\cdot\frac{\partial \varphi^*}{\partial x^*} = \frac{1}{ReSc}\left[\nabla^2\varphi^*+\frac{1}{N_{bt}}(\nabla^2 T_f^*)\right] \quad (5)$$

The dimensionless parameters are defined as follows:

$$Da=\frac{K}{H^2\varepsilon},\quad N_{bt}=\frac{D_B\varphi_0 T_1}{D_T\Delta T},\quad Sc=\frac{\mu}{\rho D_B},$$

$$Le=\frac{\alpha_f}{D_B\varphi_0},\quad Re=\frac{u_0 H}{\nu},\quad \Pr=\frac{\nu}{\alpha_f},\quad \alpha_f=\frac{k_f}{(\rho c)_f}$$

$$\tau=\frac{\varepsilon(\rho c)_p}{(\rho c)_f},\quad N_{hp}=\frac{H^2 h_{fp}}{\varepsilon(1-\varphi_0)k_f},$$

$$N_{hs}=\frac{H^2 h_{fs}}{\varepsilon(1-\varphi_0)k_f},\quad \gamma_p=\frac{(1-\varphi_0)}{\varphi_0}\frac{(\rho c)_f}{(\rho c)_p},$$

$$\gamma_s=\frac{\varepsilon(1-\varphi_0)}{(1-\varepsilon)}\frac{(\rho c)_f}{(\rho c)_s},\quad \varepsilon_p=\frac{k_p}{k_f}\frac{(\rho c)_f}{(\rho c)_p},\quad \varepsilon_s=\frac{k_s}{k_f}\frac{(\rho c)_f}{(\rho c)_s}$$

where Da, Δ, Re, Sc, Pr are the Darcy number, inertia parameter, Reynolds, Schmidt and the Prandtl numbers, respectively. The parameter Le is the nanofluid's Lewis number. τ is the modified particle-density increment and N_{bt} is a modified diffusivity ratio. This parameter can be expressed as the ratio of the Brownian diffusion to the thermophoresis diffusion. The N_{hp} and N_{hs} are the Nield numbers for the fluid/particle interface and the Nield number for the fluid/solid-matrix interface, respectively.[28–30] γ_p and γ_s are the modified thermal capacity ratios. ε_p and ε_s are the modified thermal diffusivity ratios.

Three models for the absorbed heat flux by the fluid, nanoparticles and the solid matrix are suggested for the first time as follows:

Model 1:[2] The total heat flux affected by fluid, solid and nanoparticles temperature gradient:

$$q''=\varepsilon(1-\varphi)k_f\left(\frac{\partial T_f}{\partial y}\right)_{\text{wall}}+\varepsilon(\varphi)k_p\left(\frac{\partial T_p}{\partial y}\right)_{\text{wall}} +(1-\varepsilon)k_s\left(\frac{\partial T_s}{\partial y}\right)_{\text{wall}}$$
$$\text{and}\quad T_w=T_f=T_p=T_s\quad \text{(at the impermeable wall)} \quad (6)$$

The non-dimensional heat flux is introduced as follows:

$$Q^*=\frac{q''}{k_f((T_1-T_0)/H)} \quad (7)$$

Then, the non-dimensional heat flux is introduced as:

$$Q_{m\cdot 1}^*=\varepsilon(1-\varphi^*\varphi_0)\left(\frac{\partial T_f^*}{\partial y^*}\right)_{\text{wall}}+\varepsilon(\varphi^*\varphi_0)\frac{k_p}{k_f}\left(\frac{\partial T_p^*}{\partial y^*}\right)_{\text{wall}} +(1-\varepsilon)\frac{k_s}{k_f}\left(\frac{\partial T_f^*}{\partial y^*}\right)_{\text{wall}} \quad (8)$$

$$Q_f^*=\varepsilon(1-\varphi^*\varphi_0)\left(\frac{\partial T_f^*}{\partial y^*}\right)_{\text{wall}} \quad (8\text{-}1)$$

$$Q_p^*=\varepsilon(\varphi^*\varphi_0)\frac{k_p}{k_f}\left(\frac{\partial T_p^*}{\partial y^*}\right)_{\text{wall}} \quad (8\text{-}2)$$

$$Q_s^*=(1-\varepsilon)\frac{k_s}{k_f}\left(\frac{\partial T_f^*}{\partial y^*}\right)_{\text{wall}} \quad (8\text{-}3)$$

Model 2: The total heat flux affected by solid temperature gradient:

$$q''=(\varepsilon(1-\varphi)k_f+\varepsilon(\varphi)k_p+(1-\varepsilon)k_s)\left(\frac{\partial T_s}{\partial y}\right)_{\text{wall}}\quad \text{and}\quad T_w=T_f=T_p=T_s \quad (9)$$

The non-dimensional heat flux is introduced:

$$Q_{m\cdot 2}^*=\left(\varepsilon(1-\varphi^*\varphi_0)+\varepsilon(\varphi^*\varphi_0)\frac{k_p}{k_f}+(1-\varepsilon)\frac{k_s}{k_f}\right)\times\left(\frac{\partial T_s^*}{\partial y^*}\right)_{\text{wall}} \quad (10)$$

Model 3: The total heat flux affected by fluid temperature gradient:

$$q''=(\varepsilon(1-\varphi)k_f+\varepsilon(\varphi)k_p+(1-\varepsilon)k_s)\left(\frac{\partial T_f}{\partial y}\right)_{\text{wall}}\quad \text{and}\quad T_w=T_f=T_p=T_s \quad (11)$$

The non-dimensional heat flux is:

$$Q_{m\cdot 3}^*=\left(\varepsilon(1-\varphi^*\varphi_0)+\varepsilon(\varphi^*\varphi_0)\frac{k_p}{k_f}+(1-\varepsilon)\frac{k_s}{k_f}\right)\times\left(\frac{\partial T_f^*}{\partial y^*}\right)_{\text{wall}} \quad (12)$$

Model 4: The total heat flux affected by nanoparticles temperature gradient:

$$q''=(\varepsilon(1-\varphi)k_f+\varepsilon(\varphi)k_p+(1-\varepsilon)k_s)\left(\frac{\partial T_p}{\partial y}\right)_{\text{wall}}\quad \text{and}\quad T_w=T_f=T_p=T_s \quad (13)$$

The non-dimensional heat flux can be written as:

$$Q_{m\cdot 4}^*=\left(\varepsilon(1-\varphi^*\varphi_0)+\varepsilon(\varphi^*\varphi_0)\frac{k_p}{k_f}+(1-\varepsilon)\frac{k_s}{k_f}\right)\times\left(\frac{\partial T_p^*}{\partial y^*}\right)_{\text{wall}} \quad (14)$$

where φ^* is selected as the dimensionless volume fraction of particles at the channel center.

2.1. Numerical Method

The second order finite difference method is used to solve the governing equations appeared in Eqs. (1)–(5). A fully

Table I. Grid study.

Grid number	Local Nusselt number
50∗50	7.5398
100∗100	7.5418
200∗200	7.5419
300∗300	7.542
400∗400	7.542

implicit method is employed to discretize the time dependent terms. The thermophoretic parameter, i.e., $\nabla T^* \cdot \nabla T^*$, is linearized by the method specified in Patankar.[31] The uniform grids are used in the computational domain. The results of grid independency are given in Table I. The coupled energy and volume fraction distribution equations are solved by a line-by-line iterative procedure which sweeps the computational domain in $x-y$ directions (Patankar[31]). The boundary conditions are defined as follows,

$$\begin{aligned} &\text{At } y^*=0 \text{ and } 2 \quad T_f^*=1, \quad T_p^*=1, \quad T_s^*=1, \\ &\qquad \varphi^*=0, \quad u^*=0 \\ &\text{At } x^*=0 \quad T_f^*=1, \quad T_p^*=1, \\ &\qquad T_s^*=1, \quad \varphi^*=1 \end{aligned} \tag{15}$$

For outlet boundary, the normal gradient of properties along the outlet is zero and the values of all properties at the outlet are interpolated from the computational domain.

At the channel outlet, $x^*=20$:

$$\frac{\partial T_f^*}{\partial x^*}=0, \quad \frac{\partial T_p^*}{\partial x^*}=0, \quad \frac{\partial T_s^*}{\partial x^*}=0, \quad \frac{\partial \varphi^*}{\partial x^*}=0 \tag{16}$$

The initial conditions, at $t^*=0$, are:

$$\begin{aligned} &T_f^*(t^*=0), \quad T_p^*(t^*=0), \quad T_s^*(t^*=0)=0 \\ &\qquad \text{and} \quad \varphi^*(t^*=0)=1 \end{aligned} \tag{17}$$

The computational procedure for the solution of governing equations can be summarized as follows:

1. Solve the Darcy-Brinkman equation to obtain the fluid velocity (u).
2. Use the obtained velocity and solve the fluid temperature equation to recover T_f.
3. Solve the particle temperature equation to recover T_p.
4. Solve the particle temperature equation to recover T_s.
5. Use the new values of T_f in the volume fraction distribution equation to obtain the new φ.
6. Calculate the absolute error: if $|T^{n+1}_{(f,s,p)} - T^{n}_{(f,s,p)}| > 10^{-15}$ and $|\varphi^{n+1} - \varphi^{n}| > 10^{-15}$ return to step 2 using new values of φ, T_s and T_p.

2.2. Code Validation

When the Nield number is equal to zero, the energy equations (for three phases) are completely decoupled and the obtained results are the same as one-equation model.

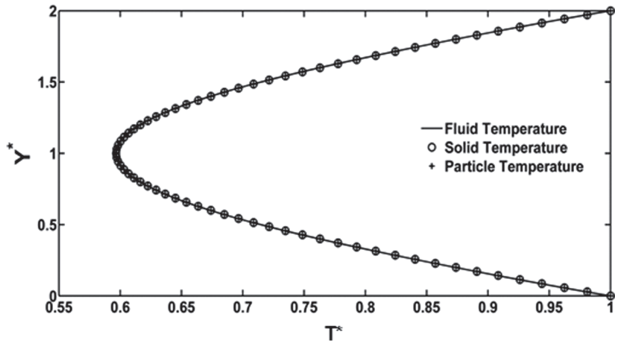

Fig. 2. Fluid temperature and solid temperature and particle temperature at $N_{hs}=10^6$ and $N_{hp}=10^6$.

In this case, the obtained results were presented in our previous work (see Maghrebi et al.[1]) and we do not repeat these results for the sake of brevity. Moreover, for checking the accuracy of numerical solution of Eqs. (3) and (4), the fluid temperature distribution in the case of thermal equilibrium is derived from our previous published paper (see Maghrebi et al.[1]) and inserted into the present code. Then, we set $N_{hs}=10^6$ and $N_{hp}=10^6$ in the simulation. As shown in Figure 2, both the solid temperature and the particle temperature distributions are fully overlapped to the fluid temperature distribution. As expected, large values of N_{hs} and N_{hp} correspond to the thermal equilibrium condition.

3. RESULTS AND DISCUSSION

In the present paper, the numerical results are related to fixed and variable values of dimensionless variables appeared in Eqs. (1)–(5) as proposed in Refs. [17], [32]–[34]. The fixed parameters are: $\varphi_0=0.03$, $N_{bt}=0.1$, $Le=100$, $Sc=100$, $\gamma_p=10$, $\gamma_s=10$, $\Pr=1$, $Re=100$, $Da=1/500$, $\tau=1$. The variable parameters are: ε_s, N_{hp} and N_{hs}.

Figure 3 displays the effect of ε_s on the temperature of the solid phase inside the porous medium. ε_s varies in the range of 1–100 ($\varepsilon_s \cong 100$ for iron-porous and water, $\varepsilon_s \cong 10$ for pyrex-porous and water and for many types of proxy and fiberglass with water as a working fluid is less than 10) for $N_{hs}=1$, $N_{hp}=1$ and $\varepsilon_p=10$. The figure

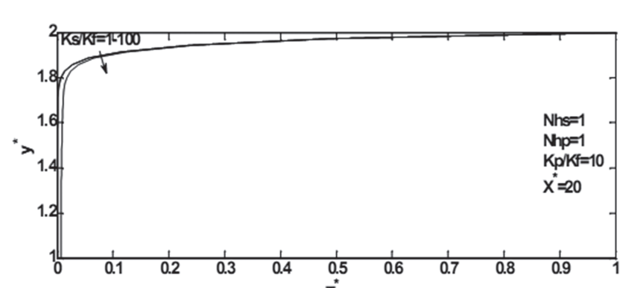

Fig. 3. Solid temperature for different values of conductivity ratio.

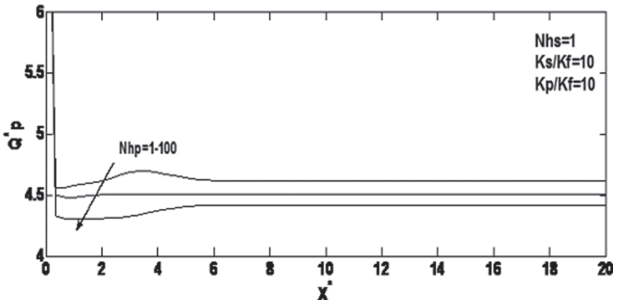

Fig. 4. Heat flux absorbed by the solid/particle phases for different values of (a) N_{hs}, (b) N_{hp}.

shows that as ε_s is increased, the temperature of the solid is also increased. However, the temperature of the solid phase does not have a visible change by increasing ε_s (from 1 to 100). The heat flux absorbed by the solid phase at the wall does not show a significant change with the conductivity ratio. A similar trend is also observed for the temperature of the particles.

The non-dimensional heat flux absorbed by the fluid phase and solid phase are investigated by Armaghani et al.[2] As shown in Figure 4, the non-dimensional heat flux absorbed by the particles is decreased by increasing N_{hp}. Owing to the decrease of the particle temperature gradient at the wall, by increasing N_{hp}, the heat flux absorbed by the particles is decreased. The absorbed heat flux by the particles in Eqs. (2)–(14) is obviously related to the temperature gradient and the nanoparticles volume fraction at the channel center. The numerical results show that the temperature gradient is the dominant term in the calculation of the particle-phase heat flux. The local increase of Q_p^* in the thermally-developing region of the channel is related to the volume fraction distribution of the particles in this region. Analyzing this interesting effect will remain for the future investigation.

Figure 5 shows the effect of different N_{hp} values on the total dimensionless heat flux for the different models 1, 2 and 3. The results indicate that the dimensionless heat flux obtained by model 1, $Q_{m\cdot 1}^*$ increases by increasing N_{hp}. By referring to Eq. (14), one can find that $Q_{m\cdot 1}^*$ is affected

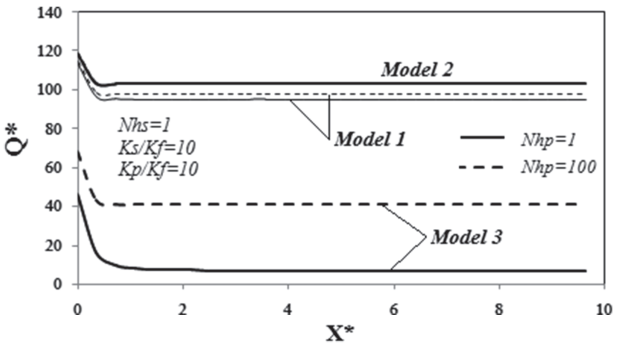

Fig. 5. Dimensionless heat flux for different values of N_{hp}.

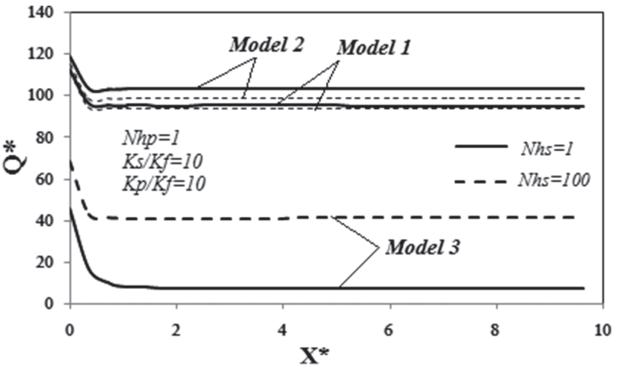

Fig. 6. Dimensionless heat flux for different values of N_{hs}.

by the fluid, solid and the nanoparticles temperature gradients at the wall. The solid temperature gradient does not have a significant effect by changing N_{hp} while the other two parameters increase with N_{hp}. As shown in this figure, the variation of N_{hp} has no significant role in changing $Q_{m\cdot 2}^*$ (dimensionless heat flux obtained by model 2). The heat flux in model 2 is only affected by the solid temperature gradient which is not sensible by N_{hp}. When N_{hp} is increased, the dimensionless heat flux obtained by model 3, $Q_{m\cdot 3}^*$ is increased. This is due to increasing of the fluid temperature gradient at the wall. The dimensionless heat flux of model 2 is greater than those obtained by the other models. As shown before, the dominant heat flux is related to that absorbed by the solid phase. One can note that model 2 is only affected by the solid temperature gradient; therefore it experienced a maximum value. Model 3 in comparison with models 1 and 2 is only affected by the fluid temperature gradient which is small with the solid-phase gradient at the wall.

Figure 6 shows the effect of various N_{hs} values on the total dimensionless heat flux. As mentioned before, $Q_{m\cdot 1}^*$ is affected by the solid, fluid and the nanoparticles temperature gradients at the wall. As discussed before, the value of Q_s^* is decreased by increasing the value of N_{hs}, while the increasing trend of Q_p^* is different from the solid-phase heat flux, as shown in Figure 4. Figure 6 clearly indicate that any decrease in Q_s^*, due to N_{hs}, does not affect the increase in Q_f^*. The results show that any increase in N_{hs} causes a decrease in the solid temperature gradient at the wall which decreases $Q_{m\cdot 2}^*$. Note that the heat flux in model 3 is only affected by the fluid temperature gradient at the wall. In this case, by increasing N_{hs}, the value of Q^* is increased.

4. CONCLUSION

In this work, we proposed and compared three new models related to heat flux of a nanofluid flowing into a porous medium-filled channel with considering thermal non-equilibrium heat transfer (please note that one model (model 1) is presented in our published paper Ref. [2]). The effects of the Nield number on the total heat fluxes

were studied and compared together. Model 2 was only affected by the solid temperature gradient; therefore it experienced a maximum value. Model 3 in comparison with models 1 and 2 was only affected by the fluid temperature gradient which was small with the solid phase gradient at the wall; therefore it experienced a minimum value.

Nomenclature

x, y Cartesian coordinate (m)
X^*, Y^* Dimensionless Cartesian coordinate ($X^* = x/H$, $Y^* = y/H$)
u Axial velocity (ms^{-1})
K Permeability (m^2)
Da Darcy number
P Pressure (Nm^{-2})
T Temperature (K)
D_T Thermophoretic diffusion coefficient (m^2s^{-1})
D_B Brownian diffusion coefficient (m^2s^{-1})
H Half length of channel (m)
t Time (s)
Re Reynolds number
Pr Prandtl number
N_{bt} Brownian motion parameter
k Thermal conductivity ($wm^{-1}K^{-1}$)
Le Lewis number
Sc Schmidt number
N_{hp} Nield number for the fluid/particle interface
N_{hs} Nield number for the fluid/solid matrix interface
h_{fp} Heat transfer coefficient between the fluid/particle
h_{fs} Heat transfer coefficient between the fluid/solid.

Greek Letters

μ Viscosity ($kgm^{-1}s^{-1}$)
ε Porosity
ρ Density (kgm^{-3})
φ Volume fraction
ε_p Modified thermal diffusivity ratio
ε_s Modified thermal diffusivity ratio
γ_p Modified thermal capacity ratio
γ_s Modified thermal capacity ratio
α Thermal diffusivity (m^2s^{-1})
τ Modified diffusivity ratio.

Subscript

s solid
f fluid
p particle
$*$ Dimensionless variables.

References and Notes

1. M. J. Maghrebi, M. Nazari, and T. Armaghani, *Transp. Porous Media* 93, 401 **(2012)**.
2. T. Armaghani, A. J. Chamkha, M. J. Maghrebi, and M. Nazari, *J. Porous Media* 17, 637 **(2014)**.
3. T. Armaghani, M. J. Maghrebi, A. J. Chamkha, and M. Nazari, *J. Nanofluids* 3, 51 **(2014)**.
4. M. Nazari, M. J. Maghrebi, T. Armaghani, and A. J. Chamkha, *Canadian J. Phys.* 92, 1312 **(2014)**.
5. S. U. S. Choi, *Development and Applications of Non-Newtonian Flows* 66, 99 **(1995)**.
6. M. A. Ismael, T. Armaghani, and A. J. Chamkha, *J. Taiwan Ins. Chem. Eng.* 59, 138 **(2016)**.
7. T. Armaghani, M. J. Maghrebi, F. Talebi, and A. B. Saryazdi, *Therm. Scie. J.* 20, 1575 **(2016)**.
8. T. Armaghani, A. Kasaeipoor, N. Alavi, and M. M. Rashidi, *J. Mol. Liq.* 223, 243 **(2016)**.
9. A. Chamkha, M. A. Ismael, A. Kasaeipoor, and T. Armaghani, *Entropy* 18, 50 **(2016)**.
10. M. H. Kayhani, H. Soltanzadeh, M. M. Heyhat, M. Nazari, and F. Kowsary, *Int. Comm. Heat Mass Transf.* 39, 456 **(2012)**.
11. X. Q. Wang and A. S. Mujumdar, *Int. J. Therm. Sci.* 46, 1 **(2007)**.
12. A. Behzadmehr, M. Saffar-Avval, and N. Galanis, *Int. J. Heat Fluid Flow* 28, 211 **(2003)**.
13. T. Armaghani, M. J. Maghrebi, and F. Talebi, *Therm. Scie. J.* 16, 455 **(2012)**.
14. M. E. M. Khedr, A. J. Chamkha, and M. Bayomi, *Model. Con.* 14, 27 **(2009)**.
15. T. Basak and A. J. Chamkha, *Int. J. Heat Mass Transfer* 55, 5526 **(2012)**.
16. A. J. Chamkha and M. A. Ismael, *International Journal of Thermal Sciences* 67, 135 **(2013)**.
17. J. Buongiorno, *ASME J. Heat transf.* 128, 240 **(2006)**.
18. M. M. Heyhat and F. Kowsary, *ASME J. Heat Transf.* 132, 062401 **(2010)**.
19. A. Baqaie Saryazdi, F. Talebi, T. Armaghani, and I. Pop, *Eur. Phys. J. Plus* 131, 78 **(2016)**.
20. D. A. Nield and A. V. Kuznetsov, *Int. J. Heat Mass Transf.* 52, 5796 **(2009)**.
21. D. A. Nield and A. V. Kuznetsov, *ASME J. Heat Transf.* 132, 052405 **(2010)**.
22. K. B. Anoop, T. Sundararajan, and K. D. Sarit, *Int. J. Heat Mass Transf.* 52, 2189 **(2009)**.
23. A. V. Kuznetsov and D. A. Nield, *Transp. Porous Media* 81, 409 **(2010)**.
24. A. V. Kuznetsov and D. A. Nield, *Transp. Porous Media* 83, 425 **(2010)**.
25. A. V. Kuznetsov and D. A. Nield, *J. Porous Media* 14, 285 **(2011)**.
26. A. V. Kuznetsov and D. A. Nield, *Int. J. Therm. Sci.* 50, 712 **(2011)**.
27. D. A. Nield, A. V. Kuznetsov, and M. Xiong, *Int. J. Heat Mass and Transf.* 46, 643 **(2003)**.
28. P. Vadasz, *ASME J. Heat Transf.* 128, 465 **(2006)**.
29. D. A. Nield, *JPM* 1, 181 **(1998)**.
30. P. Vadasz, *JPM* 15, 249 **(2012)**.
31. S. V. Patankar, Numerical Heat Transfer and Fluid Flow, Hemisphere, New York **(1980)**.
32. A. J. Chamkha, R. S. R. Gorla, and K. Ghodeswar, *Transp. Porous Media* 86, 13 **(2011)**.
33. D. A. Nield and A. Bejan, Convection in Porous Media, Springer, New York **(2013)**.
34. D. A. Nield and A. V. Kuznetsov, Effects of nanofluids on convection in porous media, chapter 14 of handbooks of porous media, Taylor and Francis Group, CRC Press, USA **(2015)**.